JPPIPA 9(10) (2023)

Jurnal Penelitian Pendidikan IPA

Journal of Research in Science Education

http://jppipa.unram.ac.id/index.php/jppipa/index

Synthesis and Characterization of PVA-Enzyme/GA/PANI-HCl Indicator Membrane Electrodes; PANI-p-toluentsulfonic acid/PVC-KTpClPB-o-NPOE, SEM-EDX, XRD and FTIR Analysis

Abd Hakim S[1*], Martha Rianna[1], Jane Elnovreny[2]

[1] Physics Department, Faculty of Mathematics and Natural Sciences, Universitas Negeri Medan, Medan, Indonesia.
[2] Industrial Engineering Study Program, Faculty of Engineering and Computer Science, Universitas Potensi Utama, Medan Indonesia.

Received: August 6, 2023
Revised: October 12, 2023
Accepted: October 25, 2023
Published: October 31, 2023

Corresponding Author:
Abd Hakim S
abdhakims@unimed.ac.id

DOI: 10.29303/jppipa.v9i10.4918

Abstract: Research has been carried out on the indicator electrode PVA-Enzyme/GA-2.9%/PPy+Sulfonic Acid/PVC-KTpClPB-o-NPOE, the amorphous spectral pattern is greatly reduced for variations of the enzyme 0.6 g in 0.5 mL (50% water + 50% alcohol) . PVA-Enzyme/GA-2.9%/PPy+Sulfonic Acid/PVC-KTpClPB-o-NPOE indicator electrode, denoted As-1. Analysis of the linear curve of the As-1 sample with a sensitivity of 41.56 mV/decade, a detection range of 10-4 - 10-1 M and a detection limit of 10-4 M, R2 = 97.51 %. To increase the sensitivity, detection range, detection limit and confidence level of R2. Indicator electrodes were made with variations of the urease enzyme on PVA and o-NPOE variations on PVC-KTpClPB 61% and 66% and replacement of PANI conductive polymer. PANI conductive polymer was dissolved in hydrochloric acid HCl denoted PANI-HCl and p-toluensulfonic acid is denoted by PANI-p-toluensulfonic acid. SEM analysis shows that the morphology of S3 is greater than that of S2. Analysis of the cps/eV EDX voltage range is greater than S3 to S2. Analysis of the XRD intensity spectrum pattern on the 2theta diffraction angle is greater than S3 to S2. Likewise, the analysis of the %Transmittance FTIR spectrum pattern for wave numbers S3, S6, S8 is higher than S2. The best result according to material analysis is S3.

Keywords: Immobilization of urease enzyme; Potentiometric biosensor; PVA-Enzyme/GA-2.9%/PANI+HCl; PANI-p-toluensulfonic Acid/PVC-KTpClPB-o-NPOE

Introduction

Modification of the indicator electrode membrane starts from; PVA-Enzyme/PVC-KTpClPB (Vlascici et al., 2012); PVA-Enzyme/GA-2.9%/PVC-KTpClPB (Aparicio-Collado et al., 2020; Vlascici et al., 2006); PVA-Enzyme/GA-2.9%/PVC-KTpClPB-o-NPOE; PVA-Enzyme/GA-2.9%/PPy+ H_2SO_4 /PVC - KTpClPB-o-NPOE, PVA-Enzymes/GA-.9%/PPy+benzenasulfonate Acid/PVC-KTpClPB-o-NPOE (Hakim S, 2023). Modification of the indicator electrode membrane aims to increase the sensitivity, detection range, detection limit and confidence level of R^2. The PVA-Enzyme/GA-2.9%/PPy+ H_2SO_4 /PVC - KTpClPB-o-NPOE indicator electrode has a sensitivity of 43.79 mV/decade, detection range of 10^{-3}-10^{-1} M, limit of detection of 10^{-3} M, R^2 = 98.83%.

The indicator electrode PVA-Enzyme/GA-2.9%/PPy+benzenasulfonic Acid/PVC-KTpClPB-o-NPOE has a sensitivity of 41.56 mV/decade, detection range 10^{-4}-10^{-1} M, detection limit 10^{-4} M, R^2 = 97.51%. These electrodes are distinguished by the type of acid in the PPy conductive polymer solvent. Based on reasoning about the type of acid in the PPy conductive polymer, the researchers made a difference in the type of acid solvent and replaced the polypyrrole (PPy) conductive

How to Cite:
Hakim, S.A., Rianna, M., & Elnovreny, J. (2023). Synthesis and Characterization of PVA-Enzyme/GA/PANI-HCl Indicator Membrane Electrodes; PANI-p-toluentsulfonic acid/PVC-KTpClPB-o-NPOE, SEM-EDX, XRD and FTIR Analysis. *Jurnal Penelitian Pendidikan IPA*, *9*(10), 8665–8671. https://doi.org/10.29303/jppipa.v9i10.4918

polymer with polyanaline conductive polymer (PANI). ModificationofPVA-Enzim/GA- .9%/PANI+HCl/PVC-KTpClPB-o-NPOE indicator electrodes are denoted S2, S5, S7; PVA-Enzim/GA-2.9%/PANI+p-toluensulfonic acid/PVC-KTpClPB-o-NPOE denoted S3, S6 and S8. Sample 2: PVA-Enzyme 1 drop/GA/PANI/HCl 6M/PVC-KTpClPB-o-NPOE 61%. Sample 5: PVA-Enzim 1 drop/GA/PANi/HCl 6M /PVC-KTpClPB-o-NPOE 66%. Sample 7: PVA-Enzim 3 drops/GA/PANI/HCl 6M/PVC-KTpClPB-o-NPOE 61%. Sample 3: PVA-Enzyme 1 drop/GA/PANI/ p-toluensulfonate 2M/PVC-KTpClPB-o-NPOE 61%. Sample 6: PVA-Enzim 1 drop/GA/PANI/ p-toluentsulfonic 2M/PVC-KTpClPB-o-NPOE 66%. Sample 8: PVA-Enzim 3 drops/GA/PANI/ p-toluensulfonate 2M/PVC-KTpClPB-o-NPOE 61%. Layer one PVA-enzyme immobilization; layer two GA crosslinks; PANI conduction polymer triple layer; and four plastesier layers of o-NPOE on PVC-KTpClPB (El-Naby, 2019).

Method

The material consists of 1.0 mm diameter tungsten 267 562 99.99%, PVA [-CH_2CHOH-]n, enzyme EC 3.5.1.5 (Urease) U4002, Glutaraldehyde (GA), PANI, HCl, p-toluensulfonic acid, PVC (CH_2CHCl)n, potassium tetrakis 4-chlorophenyl borate $(ClC_6H_4)_4BK$, tetrahydrofuran C_4H_8O, o-NPOE from sigma aldrech. The method in this study was the biosensor potentiometric method (Al-Mohaimeed et al., 2021; Bertel et al., 2021; Thakur et al., 2013)(Thakur and Ragavan, 2013); urease enzyme immobilization technique (Nimse et al., 2014)urea analyte.

GA cross-linking increases the conductivity of Hsu et al. (2022), a high-conductivity conducting polymer, enhancing electron transfer and the electrocatalytic activity of sensors (Terán-Alcocer et al., 2021). On the basis of Hakim (2021), Kaur et al. (2017), and Elbehery et al. (2019), four layers of the indicator electrode were made, each consisting of one layer with a variation of o-NPOE 61% (Hakim S, 2022) and 66% (Vlascici et al., 2006). The first layer of PVA-Enzyme one or three drops. GA second layer. The third layer is PANI-HCl and PANI-p-toluensulfonic acid. Fourth layer PVC-KTpClPB-o-NPOE, o-NPOE 61% and 66%. The products are samples S2, S5, and S7; S3, S6 and S8.

Result and Discussion

Analysis of SEM-EDX

According to figure 1, the indicator electrodes (a) one drop of PVA-E/GA/PANI-HCl/PVC-KTpClPB-o-NPOE 61%, (b) one drop of PVA-E/GA/PANI-p-toluenesulfonat/PVC-KTpClPB -o-NPOE 61%, analyzed by SEM-EDX and FTIR (Alharthi et al., 2021; Ganesan et al., 2019), SEM-EDX, XRD and FTIR analysis (Al-Mohaimeed et al., 2021; Chen et al., 2022; Ghoniem, 2016). In this session the researchers discussed SEM morphology, EDX spectral patterns and XRD spectral patterns, according to Ghoniem (2016). The EDX and XRD spectral patterns are related to the location of the working point of the indicator electrode on the Tungsten element as well as electron activity. Less crystal formation or electron activity on the indicator electrode of figure 1: PVA-E one drop/GA/PANI-HCl/PVC-KTpClPB-o-NPOE 61%, than PVA-E one drop/GA/PANI-p-toluensulfonate/PVC-KTpClPB-o-NPOE 61%. The location of the tungsten working points in the EDX spectral pattern matches the XRD spectral pattern. The location of the working point of the EDX spectral pattern at the first highest peak is in two places in Figure 2 for PANI-HCl and Figure 3 for PANI-p-toluensulfonate.

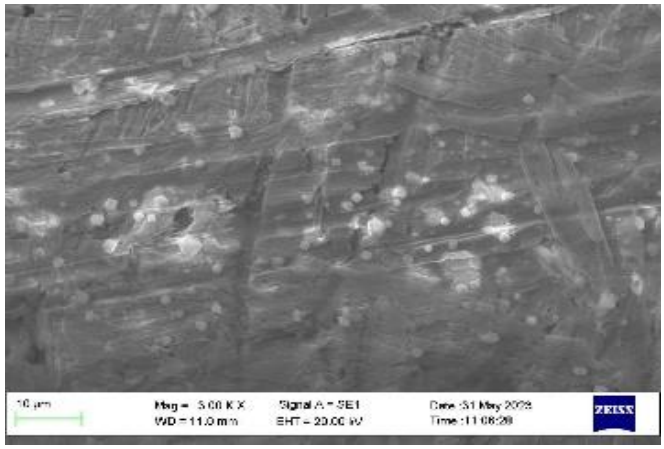

(a)

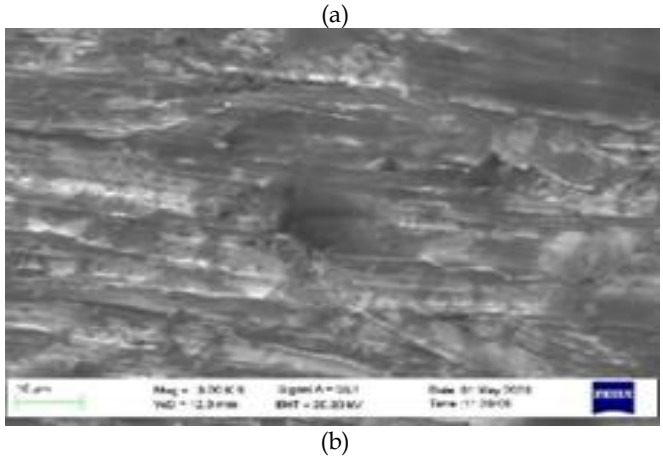

(b)

Figure 1. SEM morphology of the indicator electrode (a) one drop PVA-E/GA/PANI-HCl/PVC-KTpClPB-o-NPOE 61%, (b) one drop PVA-E/GA/PANI-p-toluensulfonate/PVC - KTpClPB-o-NPOE 61%

There are differences in morphological patterns between the indicator electrode containing PANI-HCl and PANI-p-toluensulfonate. Smaller morphology of

PANI-HCl than PANI-ptoluensulfonate. There is also the influence of the number of EDX spectrum patterns that are formed with the XRD spectrum patterns (Abbasian et al., 2016). It's just that the determination of the location of the working point is the highest peak of the EDX spectrum pattern from the supporting element of the tungsten indicator electrode. Incidentally the highest peak in the first spectral pattern from EDX Figures 2 and 3 is close to 2 keV energy, if it is connected to the XRD spectral pattern the location of the first highest peak is in sample S2 Figure 2 sample S3 Figure 4 (Joshi et al., 2021).

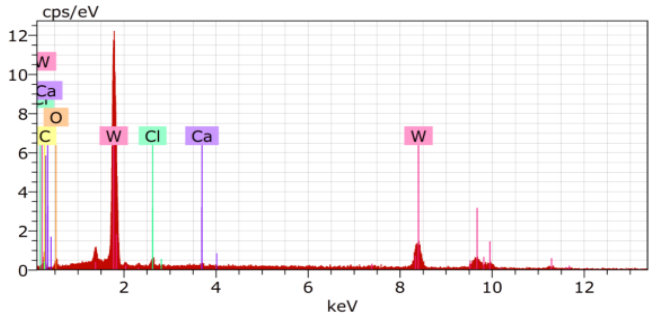

Figure 2. EDX analysis of one drop of PVA-E/GA/PANI-HCl/PVC-KTpClPB-o-NPOE 61% solution

The EDX spectrum pattern from the voltage to energy range has fewer high and low peaks in Figure 2 than in Figure 3. Where the indicator electrode is only distinguished by the difference in the third layer, namely PANI-HCl Figure 2 and PNAI-p-toluensulfonate Figure 3. Differences in spectrum patterns Figures 2 and 3 are followed by the XRD spectrum pattern in Figures 4a and 4b (Javed, A, 2021). Figure 4a and 4b are also caused by the indicator electrode in the third layer between PANI-HCl and PANI-p-toluensulfonate. More crystals were formed from the pattern of the XRD intensity spectrum at the 2theha angle in PANI-p-toluensulfonate.

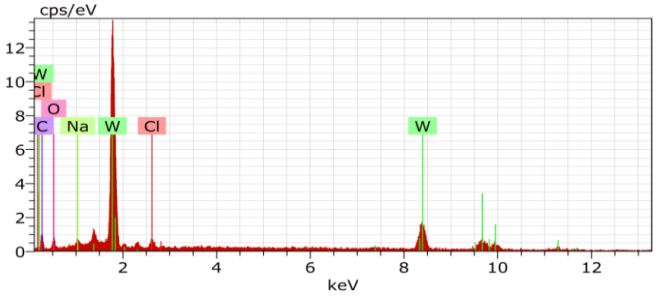

Figure 3. Analysis of the EDX PVA-E voltage range of one drop/GA/PANI-p-toluensulfonate/PVC-KTpClPB-o-NPOE 61%

The EDX spectrum pattern in the cps/eV range of voltage to energy keV is higher in the voltage range of the PANI-p-toluenesulfonate indicator electrode than the PANI-HCl voltage range. Based on these data from Figure 2 and Figure 3, p-toluensulfonic acid is better for PANI than hydrochloric acid HCl for PANI. This is also supported by the atomic weight percent of tungsten in PANI-p-toluensulfonate 76.35%wt compared to PANI-HCl 71.86%wt with the supporting elements chlorine, oxygen and carbon except for the addition of sodium to the PANI-p-toluensulfonic electrode. In PANI-HCl the supporting elements are chlorine 8.96%wt, oxygen 2.92%wt, carbon 16.26%wt. PANI-p-toluensulfonate of supporting elements chlorine 2.12%wt, oxygen 6.22%wt, carbon 14.20%wt and sodium 1.11%wt.

Table 1. Weight Percent of Indicator Electrode (a) One Drop, (b) Three Drops, PVA-E /GA/PNI-HCl/PVC-KTpClPB-o-NPOE 61%

Sample	Atomic Weight Percent				
	Tungsten	Chlorine	Oxygen	Carbon	Sodium
PVA-E satu tetes/GA/PNI-HCl/PVC-KTpClPB-o-NPOE 61%	71.86	8.96	2.92	16.26	-
PVA-E tiga tetes/GA/PNI-HCl/PVC-KTpClPB-o-NPOE 61%	76.35	2.12	6.22	14.20	1.11

XRD Analysis

The location of the working point of the XRD intensity spectrum pattern with respect to the diffraction angle 2theta (a) S2, S5 and S7, (b) S3, S6 and S8. Based on the EDX spectrum pattern according to the XRD spectrum pattern in Figure 4a table 2, samples S2 intensity 4400 (a.u), S5 1386 (a.), S7 796 (a.u) at a diffraction angle of 2theta 28.64 degrees. The XRD spectrum pattern in Figure 4b table 3 is sample S3 intensity 9451(a.u), S6 1386 (a.u), S8 5312 (a.u) at a diffraction angle of 2theta 18.2 degrees.

There are differences (Ganesan et al., 2019; Hakim S, 2021; Joshi, 2022; Shawky et al., 2021) The significant intensity of the XRD diffraction angle between the PVA-E/GA/PNI-HCl/PVC-KTpClPB-o-NPOE 61% indicator electrode and the PVA-E/GA/PNI-p-toluenesulfonate indicator electrode /PVC-KTpClPB-o-NPOE 61%. The difference between these indicator electrodes is only distinguished by the third layer, namely PANI-HCl and PNAI-p-toluensulfonate.

According to the analysis of the relationship between Figure 2 and Figure 4, it can be seen from the relationship between Figure 3 and Figure 5 that the crystalline properties of the indicator electrode with the third layer of PANI-p-toluensulfonate are more pronounced than PANI-HCl.

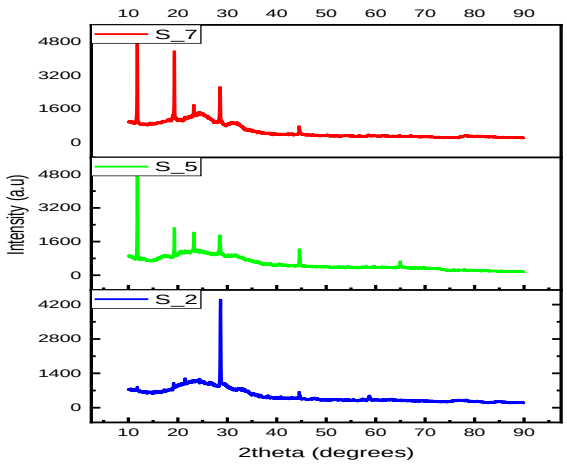

(a)

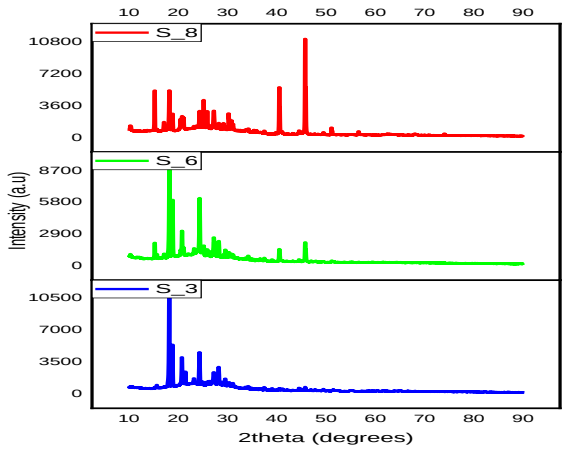

(b)

Figure 4. The pattern of the XRD intensity spectrum at 2theta diffraction angles (a) S2, S5 and S7, (b) S3, S6 and S8, (Joshi, N.C., 2022)

Table 2. Intensity Against Diffraction Angle 2theta Sample S2, S5 and S7 PVA-E/GA/PNI-HCl/PVC-KTpClPB-o-NPOE 61% Indicator Electrode

Diffraction Angle 2Theta (degrees)	HCl Intensity (a.u)		
	S2	S5	S7
11.78	846.0	4981.0	737.0
18.87	773.0	858.0	6024.0
28.64	4400.0	1386.0	796.0

The location of the PANI-HCl working point at the XRD 2theta diffraction angle is around 18.2 degrees according to the EDX spectral pattern, whereas at the diffraction angles of 11 degrees and 18 degrees are not tungsten working points for multi-layer indicator electrodes each one layer of membrane per membrane layer. Likewise, the location of the PANI-p-toluensulfonate working point is at a diffraction angle of 2theta around 28 degrees. Based on the same reasoning, the location of the PANI-p-toluensulfonate working point outside an angle of 28 degrees is not the working point of the multi-membrane PANI-p-toluensulfonate indicator electrode, each layer consisting of one layer.

Table 3. Intensity with Respect to Diffraction Angle 2theta Sample S3, S6 and S8 PVA-E/GA/PNI-p-toluensulfonate/PVC-KTpClPB-o-NPOE 61% Indicator Electrode

Diffraction Angle 2Theta (degrees)	Intensitas p-toluensulfonat (a.u)		
	S3	S6	S8
18.16	0940.0	8040.0	4855.0
18.19	9451.0	9194.0	5312.0

SEM-XRD and FTIR analysis

SEM, XRD and FTIR analysis according to Ganesan et al. (2019), Javed et al. (2021), Brini et al. (2021), Kim et al. (2020), Bibi et al. (2022), (Sanjay Krishna et al. (2019), and (Alipour et al., 2021), it is very clear the difference between the PANI-HCl indicator electrode and the PANI-p-toluenesulfonate indicator electrode. The larger pores of the PANI-p-toluenesulfonate indicator electrode, as well as crystal properties and transmittance properties starting from the wave number basins 500 – 1250 cm^{-1}, 1250 – 1750 cm^{-1} and 2750 – 4000 cm^{-1}. On the basis of SEM-EDX, XRD and FTIR the best material from a sample of one drop of PVA-E indicator electrode/GA/PANI-p-toluensulfonate/PVC-KTpClPB -o-NPOE 61% is sample S3.

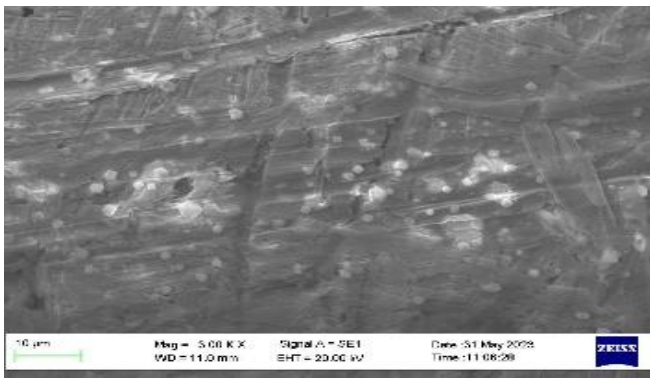

(a)

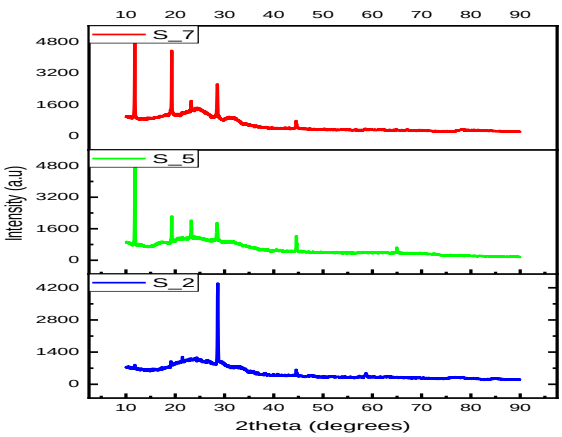

(b)

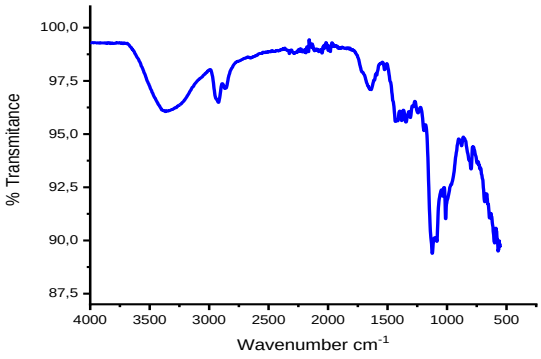

(c)

Figure 5. (a) SEM morphology, (b) XRD and (c) FTIR spectral patterns of one-drop PVA-E/GA/PANI-HCl/PVC-KTpClPB-o-NPOE 61% indicator electrodes (Wang et al., 2016)

The decision to determine the best S3 sample is supported by a larger pore, a stress range from EDX greater than 12 cps/eV, a greater percent atomic weight of 76.35 %wt, an intensity of 9451 (a.u) to a diffraction angle of 2theta 18.2 degrees, and a large number of concavity changes, reflects the many crystal patterns of the XRD spectrum pattern (Al-Mohaimeed et al., 2021; Alharthi et al., 2021; Bertel et al., 2021; Bibi et al., 2022; Chen et al., 2022).

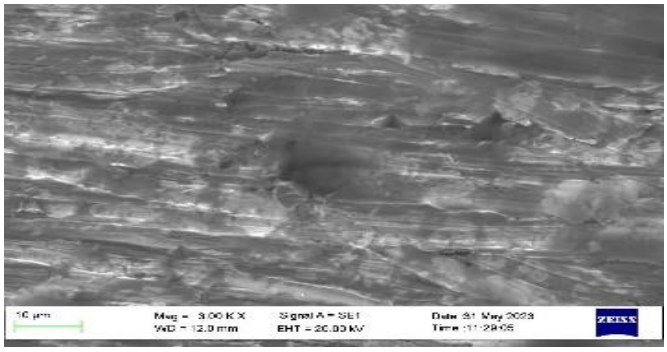

(a)

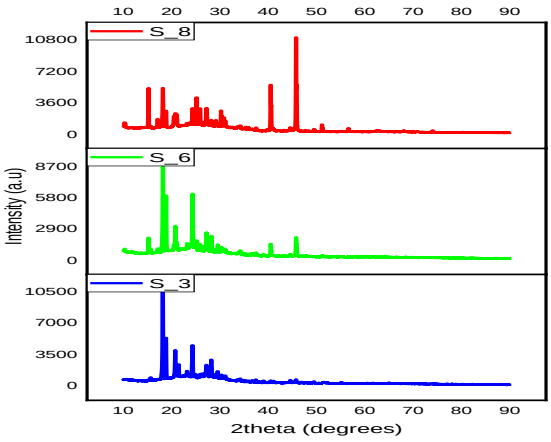

(b)

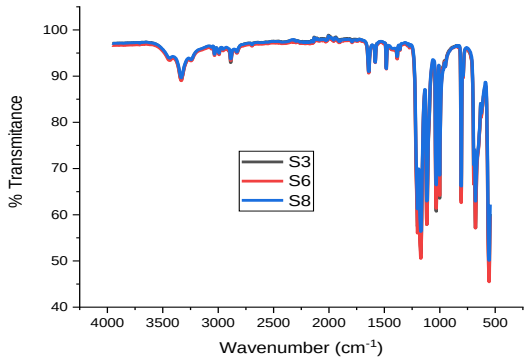

(c)

Figure 6. (a) SEM morphology, (b) XRD and (c) FTIR spectral pattern of one drop PVA-E/GA/PANI-p toluensulfonate/ PVC -KTpClPB-o-NPOE 61% (S3, S6, S8)

Conclusion

Based on the data As a conclusion from the analysis of XRD, SEM-EDX and FTIR, the best sample of the four-layer multi-membrane indicator electrode is the indicator electrode PVA-E one drop/GA/PANI-p-toluenesulfonat/PVC-KTpClPB-o-NPOE 61%.

Acknowledgements
Thanks to all parties who have supported the implementation of this research. I hope this research can be useful.

Author Contributions
Conceptualization, A. H. S., M. R., J. E.; methodology, A. H. S; validation, M. R. and J. E.; formal analysis, A. H. S; investigation, M. R, and J. E.; resources, A. H. S., and M. R.; data curation, J. E.: writing—original draft preparation, A. H. S and M. R; writing—review and editing, J. E.: visualization, and M. R. and J. E. All authors have read and agreed to the published version of the manuscript.

Funding
This research was independently funded by researchers.

Conflicts of Interest
No Conflicts of interest.

References

Abbasian, M., & Ahmadkhani, L. (2016). Synthesis of conductive PSt-g-PANi/TiO 2 nanocomposites by metal catalyzed and chemical oxidative polymerization. *Designed Monomers and Polymers*, *19*(7), 585–595. https://doi.org/10.1080/15685551.2016.1187435

Al-Mohaimeed, A. M., Mostafa, G. A. E., & El-Tohamy, M. F. (2021). New Construction of Functionalized CuO/Al2O3 Nanocomposite-Based Polymeric Sensor for Potentiometric Estimation of Naltrexone

Hydrochloride in Commercial Formulations. *Polymers*, *13*(24), 4459. https://doi.org/10.3390/polym13244459

Alharthi, S. S., Fallatah, A. M., & Al-Saidi, H. M. (2021). Design and Characterization of Electrochemical Sensor for the Determination of Mercury(II) Ion in Real Samples Based upon a New Schiff Base Derivative as an Ionophore. *Sensors*, *21*(9), 3020. https://doi.org/10.3390/s21093020

Alipour, A., Mansour Lakouraj, M., & Tashakkorian, H. (2021). Study of the effect of band gap and photoluminescence on biological properties of polyaniline/CdS QD nanocomposites based on natural polymer. *Scientific Reports*, *11*(1), 1913. https://doi.org/10.1038/s41598-020-80038-1

Aparicio-Collado, J. L., Novoa, J. J., Molina-Mateo, J., Torregrosa-Cabanilles, C., Serrano-Aroca, Á., & Sabater i Serra, R. (2020). Novel Semi-Interpenetrated Polymer Networks of Poly(3-Hydroxybutyrate-co-3-Hydroxyvalerate)/Poly (Vinyl Alcohol) with Incorporated Conductive Polypyrrole Nanoparticles. *Polymers*, *13*(1), 57. https://doi.org/10.3390/polym13010057

Bertel, L., Miranda, D. A., & García-Martín, J. M. (2021). Nanostructured Titanium Dioxide Surfaces for Electrochemical Biosensing. *Sensors*, *21*(18), 6167. https://doi.org/10.3390/s21186167

Bibi, A., Li, Y.-H., Jia, H.-W., Kuo, H., Sathishkumar, N., Chen, H.-T., Santiago, K. S., & Yeh, J.-M. (2022). Synthesis and characterization of biodegradable–electroactive polymer–Au nanocomposite materials for H2S sensing. *Express Polymer Letters*, *16*(10), 1022–1037. https://doi.org/10.3144/expresspolymlett.2022.75

Brini, L., H'Maida, K., Imgharn, A., Hsini, A., Naciri, Y., Ajmal, Z., Bouziani, A., Boulahya, A., Arahou, M., Bakiz, B., Albourine, A., & Fekhaoui, M. (2021). Synthesis and characterisation of PANI- coated Heliotrope Leaves (PANI@HL) with high clean-up capacity for Orange G dye from aqueous media. *International Journal of Environmental Analytical Chemistry*, 1–17. https://doi.org/10.1080/03067319.2021.1994557

Chen, W., Zhu, P., Chen, Y., Liu, Y., Du, L., & Wu, C. (2022). Iodine Immobilized UiO-66-NH2 Metal-Organic Framework as an Effective Antibacterial Additive for Poly(ε-caprolactone). *Polymers*, *14*(2), 283. https://doi.org/10.3390/polym14020283

El-Naby, E. (2019). Potentiometric Signal Transduction for Selective Determination of 1-(3-Chlorophenyl)piperazine "Legal Ecstasy" Through Biomimetic Interaction Mechanism. *Chemosensors*, *7*(3), 46. https://doi.org/10.3390/chemosensors7030046

Elbehery, N. H. A., Amr, A. E.-G. E., Kamel, A. H., Elsayed, E. A., & Hassan, S. S. M. (2019). Novel Potentiometric 2,6-Dichlorophenolindo-phenolate (DCPIP) Membrane-Based Sensors: Assessment of Their Input in the Determination of Total Phenolics and Ascorbic Acid in Beverages. *Sensors*, *19*(9), 2058. https://doi.org/10.3390/s19092058

Ganesan, M., Nallathambi, G., & Srinivasalu, S. (2019). Fate and Transport of Microplastics from Water Sources. *Current Science*, *117*(11), 1879. https://doi.org/10.18520/cs/v117/i11/1879-1885

Ghoniem, M. (2016). Characterization and Scientific Conservation of A Group of Archaeological Bronze Egyptian Statues. *International Journal of Conservation Science*, *7*(2), 459–476. Retrieved from https://ijcs.ro/public/IJCS-16-23_Ghoniem.pdf

Hakim S, A. (2021). Characterization of PVA-Enzyme Coated Indicator Electrodes GA coated again with PVC-KTpClPB-o-NPOE UV-Vis analysis, variable signal analysis, sensor sensitivity and SEM-EDS. *Jurnal Penelitian Pendidikan IPA*, *7*(SpecialIssue), 370–376. https://doi.org/10.29303/jppipa.v7iSpecialIssue.1248

Hakim S, A. (2022). Characterization of PVA-Enzyme Coated Indicator Electrodes GA coated again with PVC-KTpClPB-o-NPOE SEM-EDS, FTIR and XRD analysis. *Jurnal Penelitian Pendidikan IPA*, *8*(1), 103–108. https://doi.org/10.29303/jppipa.v8i1.1265

Hakim S, A. (2023). Synthesis and Characterization of PVA-Enzyme/GA/PPy/ PVC-KTpClPB-o-NPOE Indicator Electrodes, XRD Analysis, FTIR and Variable Signal Analysis. *Jurnal Penelitian Pendidikan IPA*, *9*(3), 1149–1154. https://doi.org/10.29303/jppipa.v9i3.2389

Hsu, P.-Y., Hu, T.-Y., Kumar, S., Wu, K., & Lue, S. (2022). Swelling-Resistant, Crosslinked Polyvinyl Alcohol Membranes with High ZIF-8 Nanofiller Loadings as Effective Solid Electrolytes for Alkaline Fuel Cells. *Nanomaterials*, *12*(5), 865. https://doi.org/10.3390/nano12050865

Javed, A., Abbas, S. R., Hashmi, M. U., Babar, N. U. A., & Hussain, I. (2021). Graphene Oxide Based Electrochemical Genosensor for Label Free Detection of Mycobacterium tuberculosis from Raw Clinical Samples. *International Journal of Nanomedicine*, *Volume 16*(medicine:16), 7339–7352. https://doi.org/10.2147/IJN.S326480

Joshi, N. C. (2022). Synthesis of r-GO/PANI/ZnO based material and its application in the treatment of wastewater containing Cd 2+ and Cr 6+ ions. *Separation Science and Technology*, *57*(15), 2420–2431. https://doi.org/10.1080/01496395.2022.2069042

Joshi, N. C., & Negi, S. (2021). Synthesis and adsorption potential of an organic–inorganic-based hybrid nanomaterial (PANI-Al2O3. *Inorganic and Nano-*

Metal Chemistry, *52*(3), 451–460. https://doi.org/10.1080/24701556.2021.1980026.

Kaur, H., Chhibber, M., & Mittal, S. (2017). Acyclic Arylamine-Based Ionophores as Potentiometric Sensors for Zn2+ and Ni2+ Ions. *C*, *3*(4), 34. https://doi.org/10.3390/c3040034

Kim, H., Yi, J.-Y., Kim, B.-G., Song, J. E., Jeong, H.-J., & Kim, H. R. (2020). Development of cellulose-based conductive fabrics with electrical conductivity and flexibility. *PLOS ONE*, *15*(6), e0233952. https://doi.org/10.1371/journal.pone.0233952

Nimse, S., Song, K., Sonawane, M., Sayyed, D., & Kim, T. (2014). Immobilization Techniques for Microarray: Challenges and Applications. *Sensors*, *14*(12), 22208–22229. https://doi.org/10.3390/s141222208

Sanjay Krishna, M., Balaji, S., Vadamalai Raj, G., Pravin, P. A., Sathish Kumar, M., Kothurkar, N. K., Ramani, P., Sabarish Narayanan, B., & Moorthy, A. (2019). Polymer-iron tungstate-reduced graphene oxide nanocomposites for microwave absorption. *IOP Conference Series: Materials Science and Engineering*, *577*(1), 012079. https://doi.org/10.1088/1757-899X/577/1/012079

Shawky, A. M., & El-Tohamy, M. F. (2021). Highly Functionalized Modified Metal Oxides Polymeric Sensors for Potentiometric Determination of Letrozole in Commercial Oral Tablets and Biosamples. *Polymers*, *13*(9), 1384. https://doi.org/10.3390/polym13091384

Terán-Alcocer, Á., Bravo-Plascencia, F., Cevallos-Morillo, C., & Palma-Cando, A. (2021). Electrochemical Sensors Based on Conducting Polymers for the Aqueous Detection of Biologically Relevant Molecules. *Nanomaterials*, *11*(1), 252. https://doi.org/10.3390/nano11010252

Thakur, M. S., & Ragavan, K. V. (2013). Biosensors in food processing. *J Food Sci Technol*, *50*(4), 625–641. Retrieved from https://www.ncbi.nlm.nih.gov/pmc/articles/PMC3671056/

Vlascici, D., Fagadar-Cosma, E., & Bizerea-Spiridon, O. (2006). A New Composition for Co(II)-porphyrin-based Membranes Used in Thiocyanate-selective Electrodes. *Sensors*, *6*(8), 892–900. https://doi.org/10.3390/s6080892

Vlascici, D., Fagadar-Cosma, E., Popa, I., Chiriac, V., & Gil-Agusti, M. (2012). A Novel Sensor for Monitoring of Iron(III) Ions Based on Porphyrins. *Sensors*, *12*(6), 8193–8203. https://doi.org/10.3390/s120608193

Wang, X. H., Tang, Q., Mu, Y. H., & Li, C. Q. (2016). Preparation and performance of PANI–PVA composite film doped with HCl. *Plastics, Rubber and Composites*, *45*(2), 68–71. https://doi.org/10.1080/14658011.2015.1136481